

Oscillatory migrating magnetic fields in helical turbulence in spherical domains

Dhrubaditya Mitra,¹ Reza Tavakol,¹ Petri J. Käpylä,² and Axel Brandenburg³

¹*Astronomy Unit, School of Mathematical Sciences, Queen Mary,
University of London, Mile End Road, London E1 4NS, UK*

²*Observatory, Tähtitorninmäki (PO Box 14), FI-00014, University of Helsinki, Finland*

³*NORDITA, Roslagstullsbacken 23, SE-10691 Stockholm, Sweden*

(Dated: February 12, 2019)

We perform direct numerical simulations of the compressible magnetohydrodynamical equations in a spherical shell domain with random helical forcing which has negative (positive) helicity in the northern (southern) hemisphere. We find a large-scale magnetic field, which is uniform in the azimuthal direction and shows equatorward migration. Furthermore, the large-scale magnetic field in each hemisphere oscillates on nearly dynamical time scales with reversals of polarity. We calculate the gauge-independent magnetic helicity in each hemisphere and find that they also show oscillations with the same frequency. This indicates the possible role of the exchange of helicity in these oscillations. As far as we are aware, these dynamical features of large-scale magnetic field have not been observed earlier in simulations of full magnetohydrodynamical equations.

PACS numbers: 96.60.Hv, 96.60.qd, 52.30.Cv

Many astrophysical objects, including planets and stars (and in particular our sun) possess large-scale magnetic fields with fascinating spatio-temporal modes of behavior. The polarity reversals in planetary magnetic fields and the 22 year sunspot cycle are two particularly important examples. Understanding such variations in the magnetic field is a major challenge for dynamo theory. The usual theoretical framework in which these questions are studied is that of the mean field electrodynamics [1], where the equations governing the large-scale magnetic field are obtained via Reynolds averaging of the magnetohydrodynamic (MHD) equations (see e.g., [2] for a recent review). To model these interesting dynamical features the mean field equations need to be further complemented by additional ingredients, such as the inclusion of a spatially varying coefficient of the α effect [3, 4, 5] or an imposed meridional circulation [6]. With such additional ingredients, mean field models have been shown to be able to capture a number of important spatio-temporal features of the large-scale fields observed in the sun and solar-type stars [7, 8, 9, 10]. On the other hand, simulations of the full MHD equations in most cases fail to generate large-scale magnetic fields on dynamical time scales. Typically such simulations of dynamo action use perfectly conducting boundary conditions for the magnetic field. As a result the magnetic helicity in such cases can decrease no faster than the resistive time scale and this constraint does not allow the large-scale magnetic field to reach its final saturation value at any faster rate. Some recent works overcome this constraint by using open-boundary conditions and imposed large-scale shear, see, e.g., [11, 12, 13]. Despite producing a faster growth, however, none of these cases produce oscillations in the large-scale magnetic field on dynamical time scales. Oscillatory behavior of large-scale magnetic field is found in simulations with shear and pe-

riodic boundary conditions [14, 15], although again not on dynamical time scales.

An important question is what is the minimal set of ingredients necessary to generate such interesting dynamical behaviors in large-scale magnetic field. In this paper we take a step in this direction by studying a simple model which is capable of producing a number of important features observed in sun and solar-type stars. We present direct numerical simulations of compressible MHD equations in a spherical wedge shape domain with perfectly-conducting boundary conditions. We maintain turbulence in the fluid by a random helical forcing. Also to parallel the situation in the sun we choose our forcing such that the induced kinetic helicity is negative (positive) in the northern (southern) hemisphere. We obtain growth of large-scale magnetic field beyond the equipartition value. More importantly, we observe oscillations of the magnetic field which show different polarities in different hemispheres with periodic reversals of polarity. The magnetic field develops at higher latitudes and migrates equatorward where the two different polarities of magnetic field annihilate each other and the cycle repeats as shown in Fig. 1. Such solar-like features of the large-scale magnetic field have not been observed earlier in direct simulations of MHD turbulence.

In our simulations, we write the equations for compressible magnetohydrodynamics using the magnetic vector potential \mathbf{A} , in the following way,

$$D_t \mathbf{U} = -c_s^2 \nabla \ln \rho + \frac{1}{\rho} \mathbf{J} \times \mathbf{B} + \mathbf{F}_{\text{visc}} + \mathbf{f}, \quad (1)$$

$$D_t \ln \rho = -\nabla \cdot \mathbf{U}, \quad (2)$$

$$\partial_t \mathbf{A} = \mathbf{U} \times \mathbf{B} + \eta \nabla^2 \mathbf{A}, \quad (3)$$

where $\mathbf{F}_{\text{visc}} = (\mu/\rho)(\nabla^2 \mathbf{U} + \frac{1}{3} \nabla \nabla \cdot \mathbf{U})$ is the viscous force, μ is the dynamic viscosity, $\mathbf{B} = \nabla \times \mathbf{A}$ is the

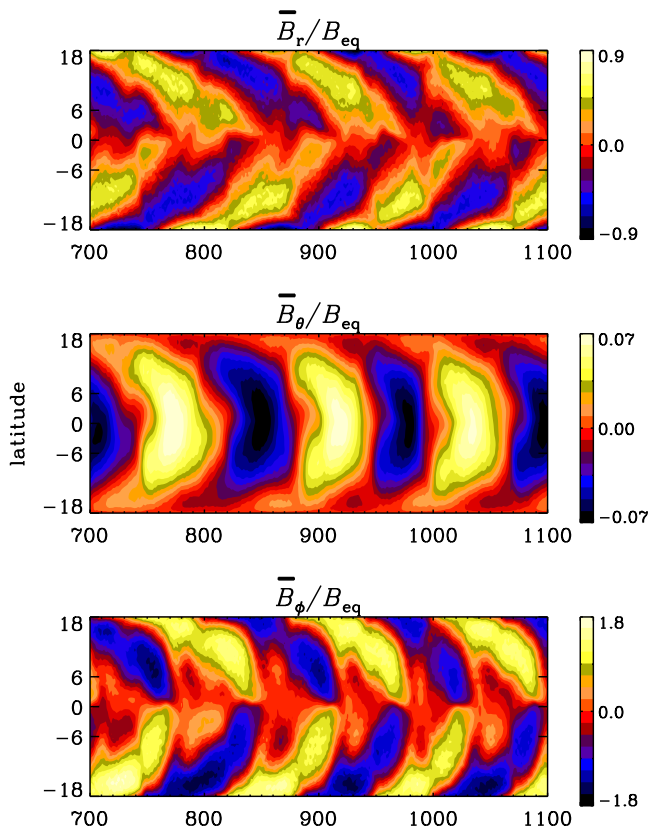


FIG. 1: Butterfly diagrams showing reversals of the polarity of large-scale magnetic field for the run S4. Shown are averaged components of the field (as defined in Eq. 4) as a function of the latitude and time. In each panel the color coding is normalized by the maximum absolute value of the corresponding component of the magnetic field.

magnetic field, \mathbf{U} is the velocity, $\mathbf{J} = \nabla \times \mathbf{B}/\mu_0$ is the current density, μ_0 is the vacuum permeability, c_s is the constant speed of sound in the medium, ρ is the density, η is the magnetic diffusivity, and $D_t \equiv \partial_t + \mathbf{U} \cdot \nabla$ is the advective derivative. Here $\mathbf{f}(\mathbf{x}, t)$ is an external random helical forcing constructed using Chandrasekhar-Kendall [16] functions as described in [17]. In this case, however, we multiply the forcing function in each hemisphere by a profile which changes sign at the equator and tends smoothly to zero at the equator from both sides. Our computational domain is a spherical wedge (see [17] for details). Motivated by the convection zone of the sun, our domain in the radial direction varies from $r_1 = 0.7$ to $r_2 = 1$ (in units of the outer radius). The azimuth (ϕ) varies from 0 to $\pi/10$ for the runs S1 and S2, and from 0 to $\pi/4$ for the runs S3 and S4. The latitude varies from $-\pi/10$ to $\pi/10$ (with the difference in latitude $\Delta\theta = \pi/5$). As an estimate of the characteris-

tic Fourier mode of the forcing we use $k_f = W_{\text{rms}}/U_{\text{rms}}$, where $W_{\text{rms}} = \langle \mathbf{W}^2 \rangle^{1/2}$ is the rms value of the vorticity, $\mathbf{W} \equiv \nabla \times \mathbf{U}$, and U_{rms} is the rms velocity. Here, angular brackets denote volume averages. We define the fluid and magnetic Reynolds numbers as $\text{Re} = U_{\text{rms}}/\nu k_f$ and $\text{Re}_M = U_{\text{rms}}/\eta k_f$, respectively. Here, ν is the kinematic viscosity given by $\nu = \mu/\rho_0$ where ρ_0 is the initial density (which is equal to the mean density throughout, noting that the mass in the volume is conserved). Details of our runs are given in table I.

Run	Grid	ν	η	Re	Re _M	k_f/k_1	ωT
S1	$32 \times 64 \times 32$	5×10^{-5}	2×10^{-5}	5	12	3	0.004
S2	$64 \times 128 \times 64$	3×10^{-5}	1.2×10^{-5}	8	21	4	0.003
S3	$32 \times 64 \times 64$	5×10^{-5}	2×10^{-5}	2	4	7	0.004
S4	$64 \times 128 \times 128$	2×10^{-5}	1×10^{-5}	4	10	7	0.004

TABLE I: Summary of our parameters including grid-size, the viscosity ν , magnetic diffusivity η (both in units of $c_s r_2$), Reynolds number Re, magnetic Reynolds number Re_M, and the cycle frequency ω_c multiplied by the time-scale T .

The large-scale magnetic field is defined via averages over the azimuthal and the radial directions, i.e.,

$$\overline{\mathbf{B}} = \langle \mathbf{B} \rangle_{r\phi}, \quad (4)$$

such that the resultant magnetic field is solely a function of the latitude. We normalize the magnetic field via the equipartition field strength which is defined by $B_{\text{eq}}^2/\mu_0 = \langle \rho \mathbf{u}^2 \rangle$. There is no unique dynamical time scale that can be used. We choose the time scale defined by the root-mean-square velocity and the smallest Fourier mode possible in our domain, i.e., $T = (U_{\text{rms}} k_1)^{-1}$ where $k_1 = 2\pi/(r_2 - r_1)$. We start our simulations with a seed magnetic field. After a transient time, we find a large-scale magnetic field is generated with energy higher than the equipartition field strength. We should note that although simulations of MHD dynamos have already been done in similar spherical wedge domains [17], these were, however, performed over only one hemisphere which included perfectly conducting boundary conditions also at the equator. Such simulations showed a slow (dissipative time scale) saturation of the large-scale magnetic field at late times. Furthermore, the large-scale magnetic field organized itself in cells of roughly unit aspect ratio along the azimuthal direction. A crucial additional feature of the present simulations is that magnetic helicity of two different signs can be exchanged across the equator.

In our simulations the generated large-scale magnetic field encompasses the whole azimuthal direction of the domain, and shows a number of novel features. The field first develops at higher latitudes and then with time migrates equatorward. Furthermore, in each hemisphere the field shows oscillations and reversals of polarity. These features can be seen in the ‘butterfly diagrams’

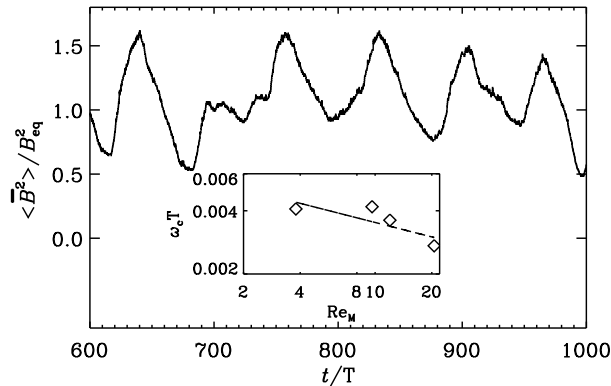


FIG. 2: Normalized large-scale magnetic energy as a function of time. The inset shows the frequency of the oscillation of the large-scale magnetic field as a function of magnetic Reynolds number, Re_M . The slope of the dashed line, which is a fit to the four points of the inset, is -0.2 .

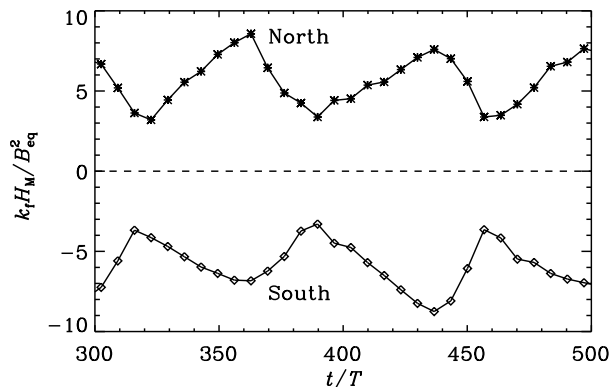


FIG. 3: Normalized gauge-independent magnetic helicity from the two hemispheres of our simulations. The frequency of oscillation is the same as that of the energy of the large-scale magnetic field.

shown in Fig. 1 where we have plotted the components of $\bar{\mathbf{B}}$ as functions of latitude and time. To further elucidate the oscillatory behavior, a plot of the normalized energy in the large-scale magnetic field as a function of time is shown in Fig. 2. The principal frequency of oscillations, ω_c , is obtained by Fourier transforming in time the time series of $\bar{B}_\phi(\theta, t)$ at a given θ ($\theta = \pi/20$ say) and selecting the frequency corresponding to the dominant mode. We have checked that this frequency does not depend on the particular value of θ chosen as long as we are not too close to the equator. The characteristic frequency of the oscillations of the large-scale magnetic energy (as shown in Fig. 2) is twice ω_c .

Given the important potential role of helicity in the generation of large-scale magnetic fields, it is important to calculate the volume averaged gauge-independent

magnetic helicity over each hemisphere in our simulations. This is a non-trivial task because the normal component of the magnetic field at the equator is not zero. For such open volumes a prescription to calculate gauge-independent magnetic helicity is as follows [18]. Let the volume V be enclosed by a surface S on which the normal component of the magnetic field is nonzero. In that case the gauge-independent magnetic helicity over this volume can be calculated as

$$H_M = \int_V (\mathbf{A} + \mathbf{A}^{\text{ref}}) \cdot (\mathbf{B} - \mathbf{B}^{\text{ref}}) dV, \quad (5)$$

where \mathbf{B}^{ref} is a reference magnetic field such that on the surface S

$$B_n^{\text{ref}} = B_n, \quad (6)$$

and inside the volume V (but not necessarily on the surface S) \mathbf{B}^{ref} is potential, i.e., generates zero current. The reference vector potential obeys

$$\nabla \times \mathbf{A}^{\text{ref}} = \mathbf{B}^{\text{ref}}. \quad (7)$$

In our case we choose \mathbf{B}^{ref} to be such that $\mathbf{B}^{\text{ref}} = 0$ everywhere in volume V and $B_n^{\text{ref}} = B_n$ on the equatorial surface. Such a \mathbf{B}^{ref} generates zero current in the volume V while at the same time satisfying the correct boundary condition. The corresponding \mathbf{A}^{ref} at a point \mathbf{x} is given as the solution of Eq. (7), which is the Biot-Savart integral, i.e.,

$$\mathbf{A}^{\text{ref}}(\mathbf{x}) = \frac{1}{4\pi} \int dx'^3 \mathbf{B}^{\text{ref}}(\mathbf{x}') \times \frac{\mathbf{x} - \mathbf{x}'}{|\mathbf{x} - \mathbf{x}'|^3}, \quad (8)$$

where in the present case this integral gives non-zero contribution only when \mathbf{x}' lies on the equatorial surface. We use this procedure to calculate the gauge-independent magnetic helicity over the northern and southern hemispheres of our simulations as shown in Fig. 3. We find that the gauge-independent magnetic helicity is positive (negative) in the northern (southern) hemisphere and oscillates with the same frequency ω_c as the large-scale magnetic energy. Note that similar oscillations in the gauge-independent magnetic helicity have also been observed in the sun [19]. However, those observations only cover the magnetic field at the scale of active regions, and not large-scale field where the magnetic helicity of a saturated dynamo is dominant and has an opposite sign [20].

Given the striking qualitative similarities of these features with those observed in the sun it is important to assess these similarities more quantitatively. Of central importance is the dependence of the cycle frequency ω_c on the magnetic Reynolds number. We have calculated the variation of ω_c as a function of magnetic Reynolds number, and the results are shown in the inset of Fig. 2. The range of magnetic Reynolds numbers probed is rather

limited. However, over this range, ω_c depends only weakly on Re_M . From the points shown in the inset of Fig. 2 we obtain a decrease of $\sim \text{Re}_M^{-0.2}$. A similar slow dependence of the oscillation period on Re_M has also been seen in other Cartesian simulations with shear [14], and may be related to a weak Re_M -dependence of the turbulent magnetic diffusivity. Simulations at larger Re_M would be desirable to see whether this Re_M -dependence eventually disappears.

To summarize, we have found large-scale magnetic fields in direct three-dimensional simulations of MHD equations with helical forcing which has two different signs of helicity at the two hemispheres. Our simulations show equatorward migration of magnetic activity as well as oscillations and polarity reversals. We further calculate the gauge-independent magnetic helicities in each hemispheric region and find they possess similar oscillations. As far as we are aware, these features have not been observed earlier in simulations of full MHD equations, although oscillations without equatorward migration have been found earlier in simulations of mean field models with spatially-varying α coefficients [3, 4, 5].

We note that in spite of the intriguing qualitative similarities of our results with the observed magnetic behavior of the sun (and solar-type stars), there are several important ingredients of the solar dynamo that are absent in this work. The most important among them is the differential rotation. Our model may have more in common with rapidly rotating stars where there is some evidence suggesting that the differential rotation is weak [22]. But even in that case there are some important differences. Although recent simulations of the MHD equations with convection and rigid rotation have yielded large-scale magnetic fields [21], it would be computationally more difficult to reproduce our results for the case of convective rigidly-rotating MHD turbulence because of the following reasons. Firstly, in our simulations there is clear scale separation between the characteristic scale of velocity and the size of the box ($k_f/k_1 = 3-7$). It generally requires much higher resolutions to achieve such scale separations in convection simulations, see e.g. [21]. Secondly, in our simulations the kinetic helicity is injected via forcing whereas in convection simulations the kinetic helicity is generated via the interaction of rotation and convection. To achieve the degree of kinetic helicity we have in our simulations (about 60 percent) in the bulk of the convection zone is likely to require more rapid rotation than in the sun. The conditions prevailing in the very deepest layers of the solar convection zone, i.e. long turnover time compared to the rotation period, might also allow 60 percent fraction of helicity.

Our aim here, however, has not been to provide a detailed model of solar dynamo which incorporates all the features known to play a role in the sun, but rather to propose a model with a small number of imposed ingredients that reproduces some of the important dynamical behavior observed in the Sun and other solar type stars. Our success here provides a step towards a better understanding of these features in solar and stellar settings.

-
- [1] F. Krause and K.-H. Rädler, *Mean-field magnetohydrodynamics and dynamo theory* (Pergamon Press, Oxford, 1980).
 - [2] A. Brandenburg and K. Subramanian, *Phys. Rep.* **417**, 1 (2005).
 - [3] F. Stefani and G. Gerbeth, *Phys. Rev. E*, **67**, 027302 (2003).
 - [4] F. Stefani and G. Gerbeth, *Phys. Rev. Lett.*, **94**, 184506 (2005).
 - [5] G. Rüdiger, D. Elstner, and M. Ossendrijver, *Astron. Astrophys.* **406**, 15 (2003).
 - [6] M. Dikpati and P. Charbonneau, *P. Astrophys. J.* **518**, 508 (1999).
 - [7] E. Covas, R. Tavakol, D. Moss, and A. Tworkowski, *Astron. Astrophys.* **360**, L21 (2000).
 - [8] E. Covas, D. Moss, and R. Tavakol, *R., Astron. Astrophys.* **429**, 657 (2005).
 - [9] M. Rempel, *Astrophys. J.* **655**, 651 (2007).
 - [10] P. J. Käpylä, M. J. Korpi, and I. Tuominen, *Astron. Nachr.* **327**, 884 (2006).
 - [11] A. Brandenburg, *Astrophys. J.* **625**, 539 (2005).
 - [12] P. J. Käpylä, M. J. Korpi, and A. Brandenburg, *Astron. Astrophys.* **491**, 353 (2008).
 - [13] D. W. Hughes and M. R. E. Proctor, *ArXiv:0810.1586* (2008).
 - [14] P. J. Käpylä, and A. Brandenburg, *ArXiv:0810.2298* (2008).
 - [15] A. Brandenburg, A. Bigazzi, and K. Subramanian, *Monthly Notice of Royal Astronomical Society.* **325**, 685 (2001).
 - [16] S. Chandrasekhar and P. Kendall, *Astrophys. J.* **126**, 457 (1957).
 - [17] D. Mitra, R. Tavakol, A. Brandenburg, and D. Moss, *ArXiv:0812.3106* (2008).
 - [18] J. Finn and T. M. Antonsen, *Comments Plasma Phys. Contr. Fusion* **9**, 111 (1985).
 - [19] M. Berger and A. Ruzmaikin, *J. Geophys. Res.* **105**, 10, 481 (2000).
 - [20] A. Brandenburg, **550**, 824 (2001), E. G. Blackman and A. Brandenburg, **584**, L99 (2003).
 - [21] P. J. Käpylä, M. J. Korpi, and A. Brandenburg, *ArXiv:0812.3958* (2008).
 - [22] R.A. Donahue, *PASP*, **105**, 804 (1993)